Materials Transactions, Vol. 42, No. 8 (2001) pp. 1552 to 1560
Special Issue on Nano-Metals I

Nanometer-Scale Structure of Rapidly Solidified $Al_{92}V_3Fe_3Zr_2$ Alloy

Tomoaki Kamiyama, Hisamichi Kimura, Kenichiro Sasamori and Akihisa Inoue

Institute for Materials Research, Tohoku University, Sendai 980-8577, Japan

Nanometer-scale structures were examined for $Al_{92}V_3Fe_3Zr_2$ ribbons rapidly solidified by a single roller melt-spinning, as a function of a circumferential velocity in the range between 10 and 50 m/s. Deformed scattering patterns along the direction of the ribbons are detected by a pinhole small-angle X-ray instrument for the ribbons rapidly solidified with the circumferential velocities higher than 20 m/s. The deformed patterns can be attributed to the rows of nearly spherical particles into which the elongated particles have disintegrated by shear flow caused by the melt spinning. Size of precipitates decreases with increasing the circumferential velocity, and some change in the precipitation mechanism is suggested to occur at a circumferential velocity of 30 m/s.

(Received February 21, 2001; Accepted March 28, 2001)

Keywords: *small-angle X-ray scattering, nano-structure, melt-spinning, shear, aluminum-based amorphous alloy*

1. Introduction

Aluminum-based amorphous alloys with excellent mechanical strengths have been developed by Inoue *et al.* using rapid solidification. The microstructures of the Al-based alloys were clarified to consist of amorphous particles 3 to 10 nm in diameter in an fcc-Al matrix in many cases, and to be responsible for their high strength.[1] Sizes of the precipitates may be kept within nano-meter length scales during nucleation, probably due to the relatively low precipitation temperature of aluminum metal and low growth rate of the non equilibrium phases occurring frequently in the crystallization process of amorphous phase.[2]

A nonequilibrium structure consisting of nanoscale amorphous particles surrounded by fcc-Al phase was found to be formed in an $Al_{94}V_4Fe_2$ alloy by melt spinning with a circumference velocity of 40 m/s; while deviations from these alloy component and solidification condition lead to the formation of the nanoscale mixed structure of Al+icosahedral (I) phases or Al+I+amorphous phases.[3] From these results, Inoue *et al.* proposed that the formation of the nanoscale amorphous particles in coexistence with Al phase is due to the suppression of the transition from super-cooled liquid to I-phase resulting from the retardation of the diffusivity of the solute elements vanadium and iron.[3]

Kavesh demonstrated that the ribbon formation in the melt spinning method can be described in terms of the transport dominated mode that the ribbon is formed by transport of momentum and/or heat between the melt puddle and the chill surface (Fig. 1).[4] He also described that thermal propagation is roughly three to nine times faster than momentum propagation for the metallic liquid; and a solid boundary layer will form adja-cent to the chill surface and propagate into the melt puddle to form the ribbon.[4] As materials within the solid layer move with the velocity of the chill surface, the high shear rate S in the thin boundary layer of fluid can be obtained by melt-spinning with a high circumference velocity of the chill surface.

The density-density correlation function should experience significant distortions if the Deborah number $D = S\tau$ becomes comparable to one, where τ is the longest characteristic structural relaxation time.[5] It should be noted in passing that the characteristic relaxation time τ for chain deformation is of order $\eta R_g^3/k_BT$ for a single polymer,[6] where R_g is the radius of gyration and η is the solvent viscosity. Large R_g implies large τ in this case. So far, nucleation in shear has been studied regarding polymers in dioctylphthalate or aqueous solution *etc.*, mainly by means of light scattering.[7] For example, Min and Goldburg[8] investigated nucleation of a supercooled binary fluid mixture (lutidine and water) exposed to uniform steady-state shear S, and observed that the shear ruptures all droplets exceeding a certain size, $R = R_{burst}$. According to Min *et al.*, when S is relatively low so that R_{burst} exceeds the critical radius R_c, the system achieves a steady state. Under strong shear, where R_{burst} is very close to R_c, all the existing droplets suddenly disappear.[8]

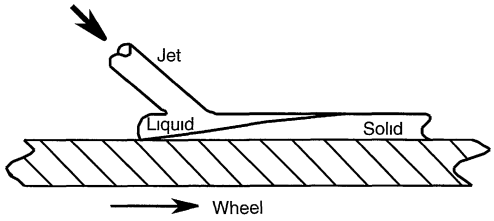

Fig. 1 Schematic illustrating ribbon formation process during single roller melt-spinning.[4]

Relatively long time for the transition from supercooled liquid to I-phase compared to that of the formation of the nanoscale amorphous particles makes us presume the strong dependence of the microstructures on the circumference velocity 40 m/s of the chill in the Al-based liquid alloys containing elements vanadium and iron. That is, if the relaxation time τ and the shear rate S are large enough to achieve a relation $S\tau \cong 1$, the microstructures with nano-scale fluctuations in density or composition are expected to be distorted by melt-spinning depending on the circumference velocity.

Small-angle X-ray scattering (SAXS) techniques have been used for making structural characterization of materials for length scales between 1 and 100 nm.[9] A SAXS measurement using a point-collimated instrument with an area detector leads to a direct detection of deformed scattered intensity and enables us to detect even a slightly deformed scattering

pattern.

The formation of nanometer-scale precipitates in Al-based amorphous alloys prepared by the rapid solidification method was examined by SAXS techniques in this work, as a function of circumference velocity of melt-spinning, in order to clarify the effects of the melt spinning on the formation mechanism of the microstructure in the Al-based alloys. Some features of the SAXS examination were outlined previously at the NANO2000 meeting in Sendai 2000.[10] In the present paper, a more precise description will be given.

2. Experimental Procedures

A quaternary Al–V–Fe–Zr alloy containing V and Fe as solute elements was prepared for the present study, along with an Al–Cr–Ce–Co alloy. Rapidly solidified $Al_{92}V_3Fe_3Zr_2$ ribbons were prepared by a single roller melt-spinning with circumference velocities (V_c) of 10, 20, 30, 40 and 50 m/s. Ribbons with another composition of $Al_{94.5}Cr_3Ce_1Co_{1.5}$ were prepared at V_c of 40 m/s. Compositions are nominally expressed in atomic percent. The details of their preparation procedures and characteristic features have been described in the works of Inoue *et al.*[1]

Figure 2 illustrates the overall drawings of the pinhole SAXS instrument utilized in this study. The collimation, sample and detection housings are mounted on rails as shown in this figure, for the instrumental geometry to be set readily in accordance with the length scale of structural inhomogeneities to be detected. A 18 kW rotating-anode X-ray source mounted on a goniometer produces a monochromatized X-ray beam in combination with a graphite crystal. The monochromatized beam is reflected by a Pt-coated silica mirror and collimated with two pinhole apertures (0.5 mm × 0.5 mm and 0.3 mm × 0.3 mm) separated by 800 mm. The higher-order harmonics of copper Kα radiation is eliminated.

The scattered radiation was recorded as two-dimensional data (used pixel size 0.3 mm × 0.3 mm) on the imaging plate fixed by a beam stop in detector chambers. The imaging plate can be positioned at three different distances from the sample, in detector chambers 1, 2 and about 7.2 mm apart from the sample in the sample chamber, to give an effective q range of about $0.07 < q < 35\,\mathrm{nm}^{-1}$ for the same instrumental geometry. The modulus of scattering vector $\boldsymbol{q}$, which is given by $q = 4\pi \sin\theta/\lambda$, λ is the wave length of the incident radiation and 2θ is the scattering angle, was determined from the ring corresponding to the Bragg reflection in the scattered intensity from stearic acid or Si powder. The resolutions of the apparatus for Cu-Kα radiation were $\Delta q_{\mathrm{FWHM}} \cong 0.05\,\mathrm{nm}^{-1}$ for the detector positioned in detector chamber 2 and $\cong 0.25\,\mathrm{nm}^{-1}$ for that in the sample chamber, estimated from peaks in the scattered intensities from bovine collagen and Si powder, respectively. All the flight paths including the specimen chamber were evacuated to a pressure of 1 Pa. With the setting of the imaging plate in evacuated chambers, measurements are free from the corrections that would result from the use of a large size exit window.

All the SAXS measurements on the Al-base ribbons were performed at room temperature on a pinhole SAXS instrument with experimental geometries as illustrated in Fig. 3 using Cu-Kα radiation. The specimens for SAXS measurements were prepared in the form of a bundle about 70 μm in effective thickness by stacking the ribbons of thickness about 20 μm in one direction.

The scattering data obtained by the circular or sector average of the measured two-dimensional data were corrected only for background and the absorption. Correction for background from noises originating from the read-out system of the imaging plate is required especially in the measurements of this type. A region shielded from the scattered X-rays was prepared on the imaging plate and the corrections were made by subtracting the intensity recorded in this region from the scattering intensity in the region irradiated with scattered X-rays. Noises of this type were eliminated to a great extent by this subtraction. Since the sample for X-ray measurements was in the form of a bundle consisting of the ribbons about 1 mm in width, samples of precisely uniform thickness could not be prepared and the scattering data were not corrected for sample thickness in this work. Statistical errors for the scattering data were determined by the evaluation of the square root of the variance obtained in the calculation of circular or

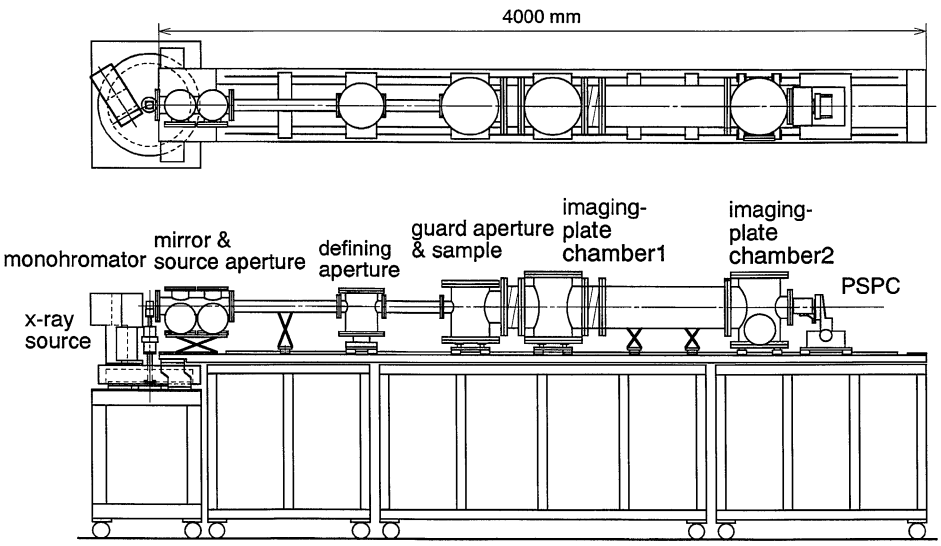

Fig. 2 Schematic representations of the pinhole small-angle X-ray instrument.

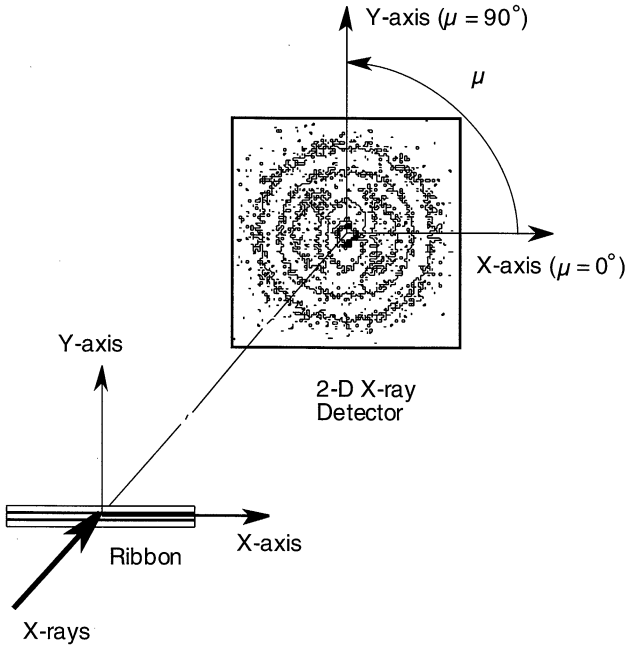

Fig. 3 Geometry of the SAXS measurement of amorphous ribbons. Azimuthal angles $\mu = 0°$ and 180° correspond to the direction of the ribbon.

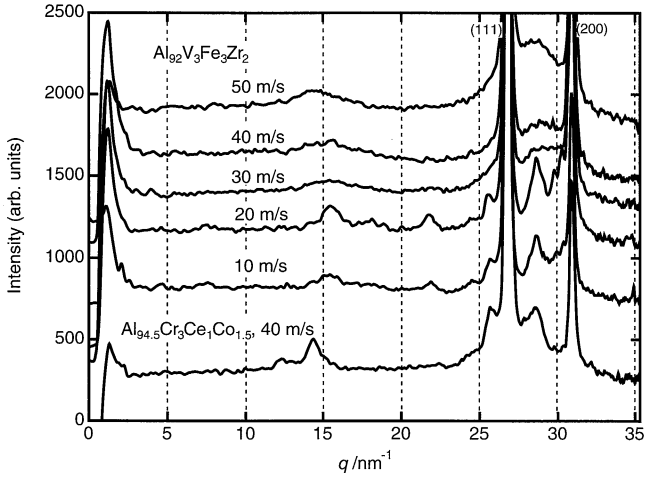

Fig. 4 X-ray diffraction patterns of melt-spun $Al_{92}V_3Fe_3Zr_2$ ribbons prepared at different circumferential velocities between 10 and 50 m/s, along with the melt-spun $Al_{94.5}Cr_3Ce_1Co_{1.5}$ ribbon prepared with 40 m/s.

sector averaging.

3. Results

3.1 Results of measurements

The X-ray diffraction patterns of the $Al_{92}V_3Fe_3Zr_2$ alloy prepared at different V_c values between 10 m/s and 50 m/s are presented in Fig. 4, along with that of the $Al_{94.5}Cr_3Ce_1Co_{1.5}$ alloy prepared with V_c of 40 m/s. For the $Al_{94.5}Cr_3Ce_1Co_{1.5}$ alloy, the diffraction peaks were shown previously by Inoue *et al.*[1] to consist of fcc-Al and icosahedral (I) phases. As the diffraction peaks in the scattering profiles from the $Al_{92}V_3Fe_3Zr_2$ alloy prepared at V_c of 10 m/s and 20 m/s coincide in position with those from the $Al_{94.5}Cr_3Ce_1Co_{1.5}$ alloy, the diffraction peaks for the $Al_{92}V_3Fe_3Zr_2$ alloy can be attributed also to the fcc-Al and I phases prepared with V_c of 10 m/s and 20 m/s. At V_c values higher than 30 m/s, a broad diffraction peak is observed in the q region where the reflection peaks corresponding to the I phases are expected, in addition to the diffraction peak from an fcc-Al phase. The broad peak becomes more distinct with increasing V_c value to 50 m/s.

Transmission electron micrographs (TEM) for the $Al_{92}V_3Fe_3Zr_2$ alloy shown in Fig. 5 demonstrate that the microstructure of the ribbons consists of precipitates with diameters of about 50, 40 and 17 nanometers in nearly close contact with each other, for the ribbons prepared at the V_c values of 10, 20 and 40 m/s, respectively.

The scattered intensities recorded on the two-dimensional position-sensitive detector were plotted in Fig. 6 in the form of isointensitiy contour maps for the melt-spun $Al_{92}V_3Fe_3Zr_2$ alloys as a function of circumferential velocity, along with the $Al_{94.5}Cr_3Ce_1Co_{1.5}$ ribbons prepared at 40 m/s. The azimuthal scattered intensities obtained from the two-dimensional data are plotted in Fig. 7, in order to demonstrate the deformation

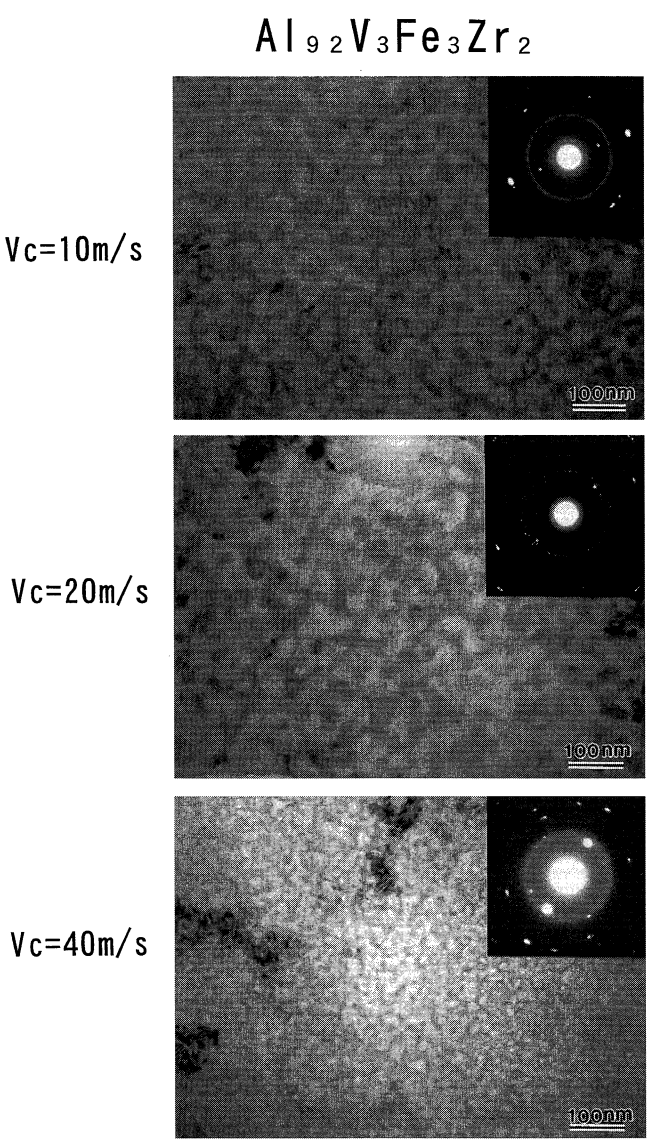

Fig. 5 Bright-field electron micrographs and selected area electron diffraction patterns of melt-spun $Al_{92}V_3Fe_3Zr_2$ ribbons peppered at circumferential velocities 10, 20 and 40 m/s.

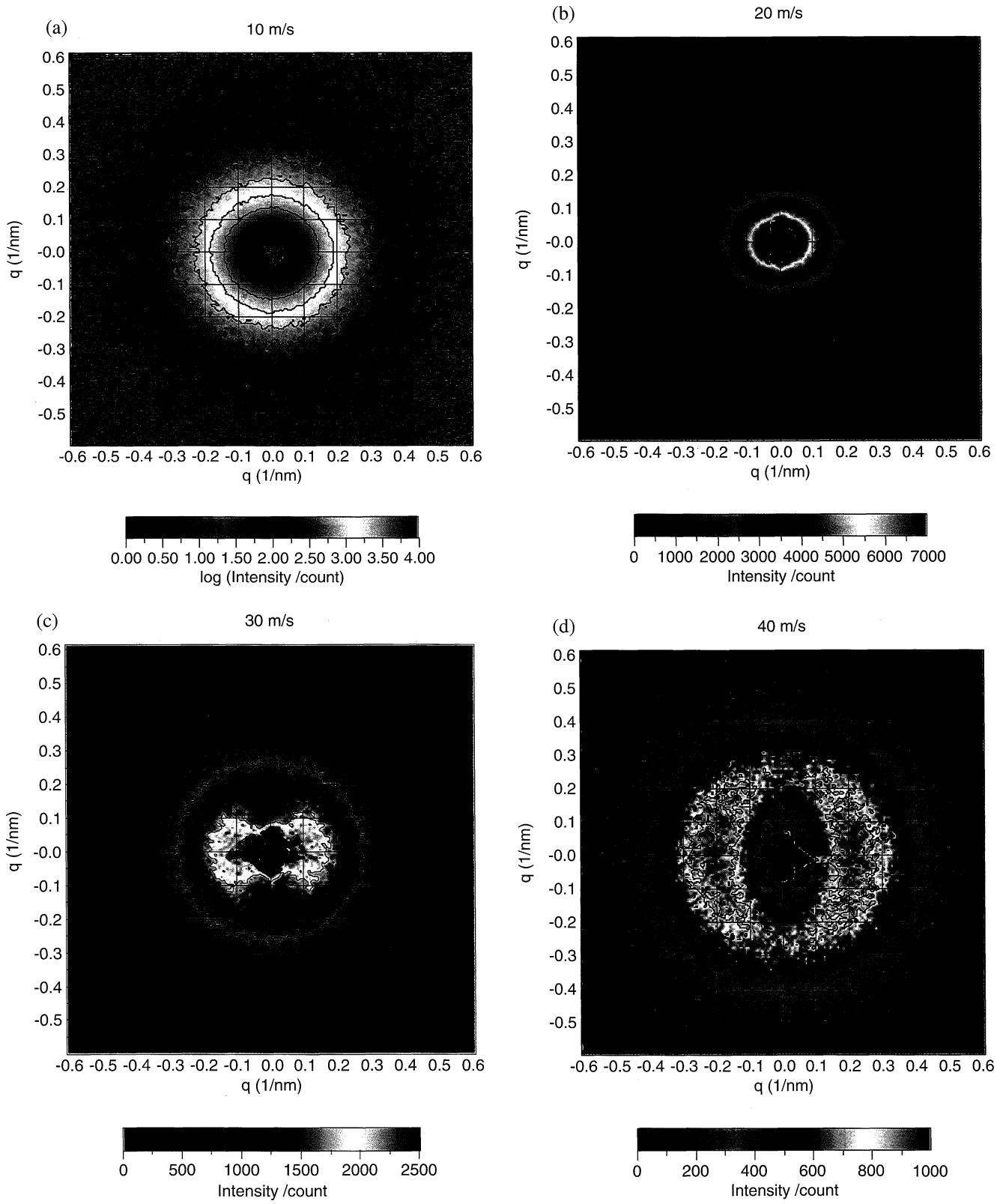

behavior clearly.

Features of the SAXS patterns can be described as follows.

i) Deformed SAXS patterns were detected on the area detector for the $Al_{92}V_3Fe_3Zr_2$ ribbons prepared at circumferential velocities V_c higher than 20 m/s. An isotropic pattern was observed for the $Al_{92}V_3Fe_3Zr_2$ ribbon prepared at V_c of 10 m/s and the $Al_{94.5}Cr_3Ce_1Co_{1.5}$ ribbon prepared with V_c of 40 m/s.

ii) All the distorted isointensity curves are oriented along the direction of ribbons in the low q region below $q \approx 0.3\,nm^{-1}$, and they become isotropic in the q region above about $0.3\,nm^{-1}$.

iii) The circularly averaged scattering curves decay following q^{-4}, the Porod law, in the large q region where

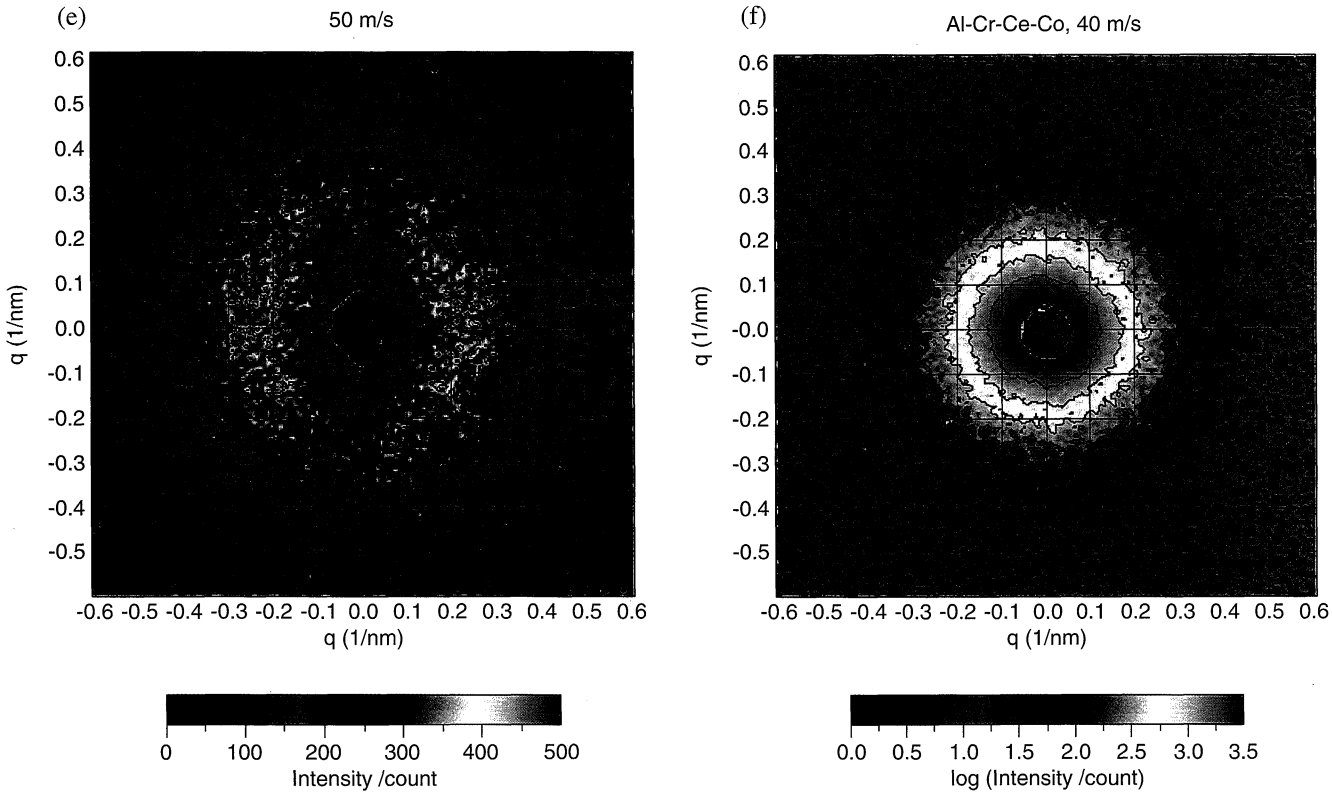

Fig. 6 Two-dimensional scattering patterns in the form of an isointensity contour map for melt-spun $Al_{92}V_3Fe_3Zr_2$ ribbons prepared at circumferential velocities of 10, 20, 30, 40 and 50 m/s and $Al_{94.5}Cr_3Ce_1Co_{1.5}$ ribbons prepared with 40 m/s. Intensities for the $Al_{92}V_3Fe_3Zr_2$ ribbons with 10 m/s and the $Al_{94.5}Cr_3Ce_1Co_{1.5}$ ribbons are logarithmically spaced. The direction of the ribbon is horizontal.

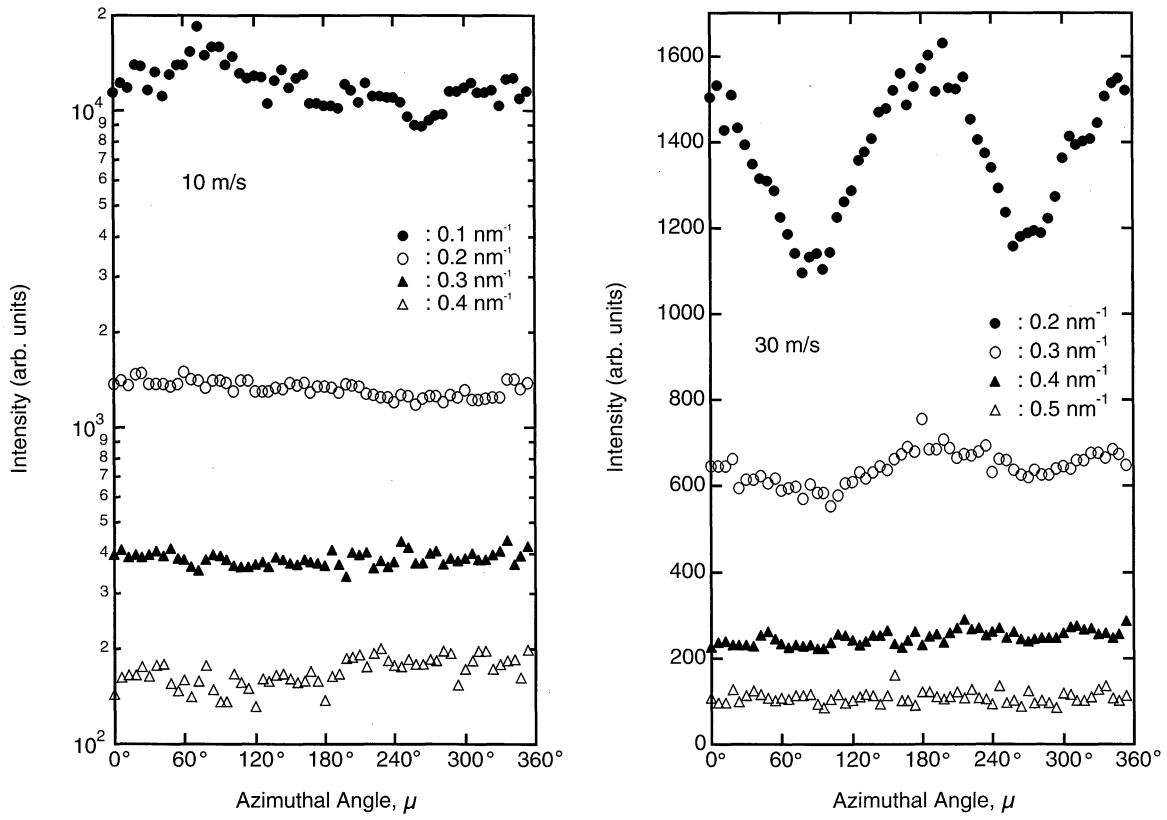

Fig. 7 Azimuthal scattered intensity at constant q positions calculated from the two-dimensional scattering pattern for melt-spun $Al_{92}V_3Fe_3Zr_2$ ribbons prepared at circumferential velocities 10 and 30 m/s. Azimuthal angles $\mu = 0°$ and 180° are the direction of the ribbon.

the isointeisity curves become circularly symmetric, for the $Al_{92}V_3Fe_3Zr_2$ alloy prepared at V_c higher than 30 m/s, while the decays of the scattering curves of the $Al_{92}V_3Fe_3Zr_2$ alloy prepared at V_c less than 20 m/s and the $Al_{94.5}Cr_3Ce_1Co_{1.5}$ ribbons deviate clearly from the Porod law. This shows that the scattering is caused by precipitated particles with a well-defined boundary in a medium for the ribbons prepared at V_c higher than 30 m/s, and the absence of distinct interface for the $Al_{92}V_3Fe_3Zr_2$ alloy prepared at V_c less than 20 m/s and the $Al_{94.5}Cr_3Ce_1Co_{1.5}$ alloy.

iv) An increase in the V_c value from 10 to 20 m/s changes the isotropic SAXS pattern of the $Al_{92}V_3Fe_3Zr_2$ alloy into distorted patterns, and the increase from 30 to 50 m/s gives rise to the development of well defined maxima in the SAXS patterns and causes a shift in the peak positions toward larger q. The deformed rings of diffuse maxima in the two-dimensional scattering data are well approximated by an ellipse whose principal axes are 0.21 ± 0.01 and $0.25 \pm 0.01\ nm^{-1}$ parallel and perpendicular to the direction of the ribbon, respectively, for $Al_{92}V_3Fe_3Zr_2$ alloy prepared with V_c of 40 m/s (Fig. 8(a)), and are 0.22 ± 0.01 and $0.28 \pm 0.01\ nm^{-1}$ for 50 m/s. An azimuthal scattered intensities along the estimated ellipse for the $Al_{92}V_3Fe_3Zr_2$ alloy prepared with V_c of 40 m/s are illustrated in Fig. 8(b).

In the present work, all the fitting or approximation procedures were performed using a modified Marquardt method in the SALS system.[11]

3.2 Analysis of the SAXS data

A typical deformed patterns for the $Al_{92}V_3Fe_3Zr_2$ alloy prepared with V_c of 40 m/s is represented in Fig. 9, in the form of sector-averaged scattered intensities along with circularly averaged intensity. Scattered intensities exhibit maxima for the $Al_{92}V_3Fe_3Zr_2$ alloys prepared with V_c values of 40 and 50 m/s, as shown in Fig. 9. The TEM observation showed that the microstructure consists of precipitates of approximately spherical particles with a diameter of about 17 nm which are dispersed in nearly close contact with each other for the $Al_{92}V_3Fe_3Zr_2$ alloy prepared with V_c of 40 m/s. The effect of interparticle interference must be taken into account for the interpretation of the maxima in the scattered intensities.

Therefore, it is considered to be reasonable from the TEM observation that the approximately spherical particles are dispersed, to interpret the scattered intensities in terms of an equation

$$I(q) = nP(q)S(q), \tag{1}$$

which holds in the system which contains a monodisperse population of spherical scatterers, where n is the number density of spheres, $P(q)$ is the particle form factor and $S(q)$ is the structure factor for the correlation between particles. The scattered intensity in the larger q where the isointeisity curves are circularly symmetric can be attributed largely to the contribution from the form factor $P(q)$, because the form factor reflects the shape of the particle and the distribution of atomic species within it. This consideration enables us to attribute the distorted patterns and the maxima to the structure factor $S(q)$.

As the isotropic parts of the scattered intensities can be attributed to the form factor $P(q)$ predominantly, the Guinier approximation[9]

$$I(q) = \text{const} \cdot \exp(-R_g^{2/3}), \tag{2}$$

where R_g is the radius of gyration of the particle, can be applied to the smaller q parts of the isotropic scattered intensities. Figure 10 shows the Guinier plots for the $Al_{92}V_3Fe_3Zr_2$ ribbons, and gives the radii of gyration 25.2 ± 1.2, 14.8 ± 0.5, 6.77 ± 0.16, 5.37 ± 0.17 and 4.38 ± 0.21 nm at V_c values of 10, 20, 30, 40 and 50 m/s, respectively. The scattered intensities are described well by the Guinier approximation for the $Al_{92}V_3Fe_3Zr_2$ alloy prepared with V_c values higher than 30 m/s. While, the Guinier regions where the scattered in-

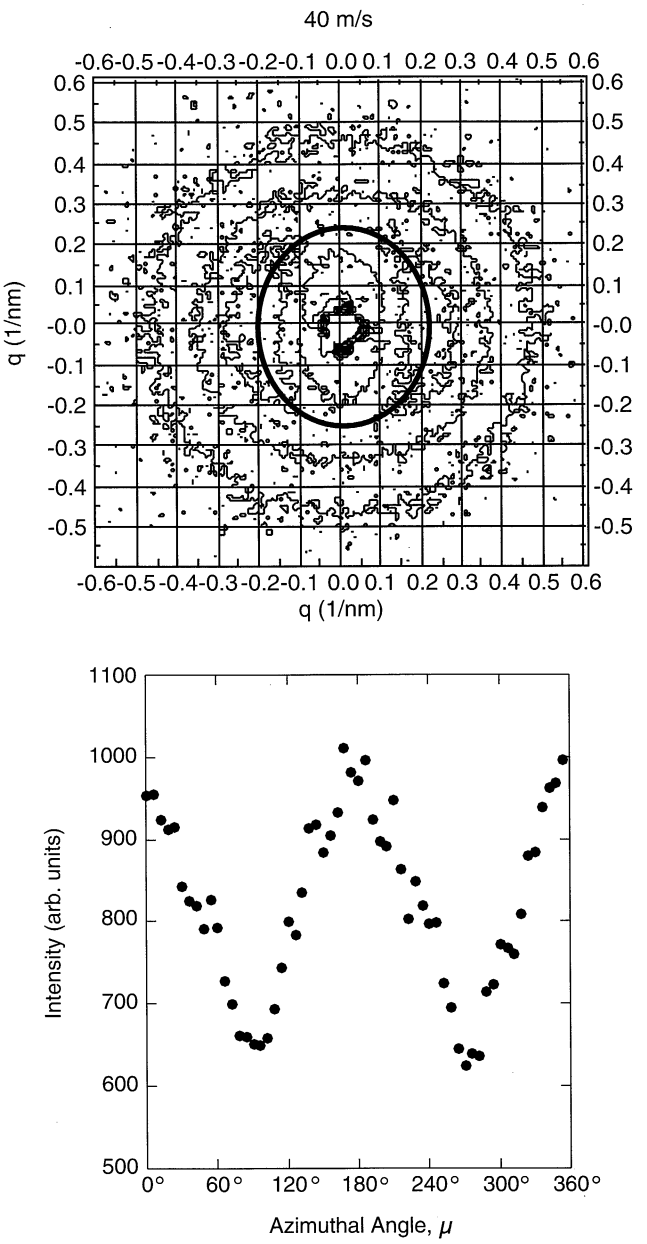

Fig. 8 (a). The deformed ring of diffuse maxima in the two-dimensional scattering data approximated by an ellipse whose principal axes are 0.21 and $0.25\ nm^{-1}$ parallel and perpendicular to the direction of the ribbon, together with an isointensity contour map for melt-spun $Al_{92}V_3Fe_3Zr_2$ ribbon prepared at a circumferential velocity of 40 m/s. (b). Azimuthal scattered intensity along the ellipse drawn in Fig. 8(a) for melt-spun $Al_{92}V_3Fe_3Zr_2$ ribbon prepared at a circumferential velocity of 40 m/s.

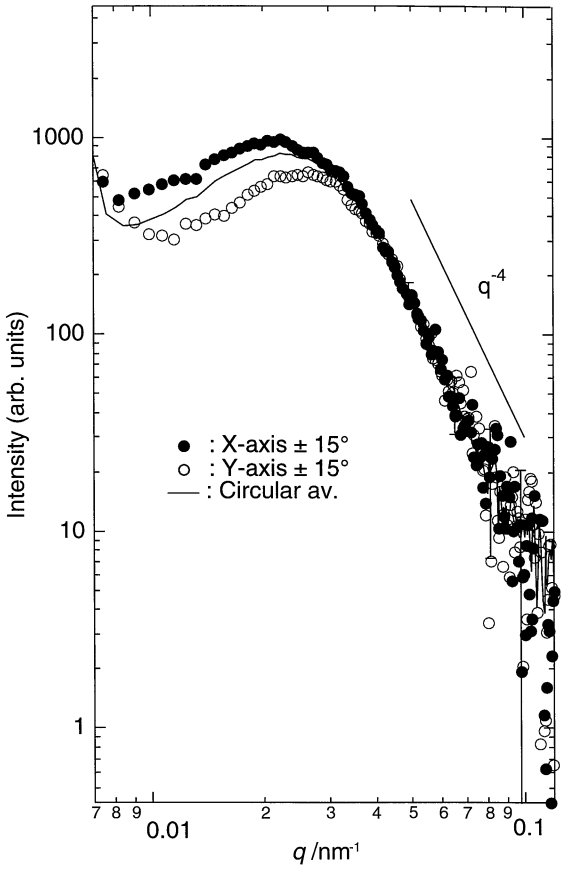

Fig. 9 The sector-averaged scattered intensities for melt-spun $Al_{92}V_3Fe_3Zr_2$ ribbon prepared at a circumferential velocity of 40 m/s, together with circularly averaged intensity.

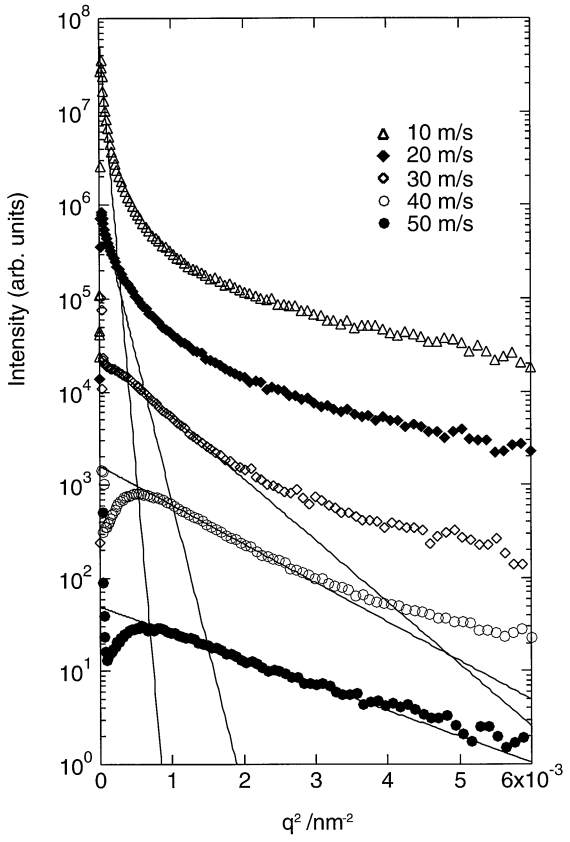

Fig. 10 Guinier approximation fits for $Al_{92}V_3Fe_3Zr_2$ ribbons prepared at circumferential velocities of 10, 20, 30, 40 and 50 m/s.

tensities are approximated well by eq. (2) are narrow for the ribbons prepared with V_c of 10 and 20 m/s, presumably owing to polydispersity effects.

4. Discussion

The formation mechanisms of the $Al_{92}V_3Fe_3Zr_2$ alloy during the melt spinning process are discussed on the basis of the transport dominated mode given by Cavesh.[4] According to Schlichting,[12] the depth of penetration of thermal and momentum effects in a fluid near a solid-liquid boundary is given by

$$\frac{\delta\tau}{\delta_M} \sim (Pr)^{-1/2} \tag{3}$$

where Pr is the Prandtl number of the fluid, δ_T is the thermal boundary layer, and δ_M is the momentum boundary layer thickness. If the thermal boundary layer δ_T is replaced approximately by the ribbon thickness, say 20 μm, the boundary layer thickness $\delta_M = 3.5\,\mu m$ in the fluid is estimated from the value 5.7 of δ_T/δ_M for liquid aluminium at 873 K[4] using eq. (3). This predicts that the shear rates S of 3–14 × 10^6 s^{-1} at the boundary layer of the $Al_{92}V_3Fe_3Zr_2$ alloy will be achieved by the melt-spinning corresponding to V_c values from 10 to 50 m/s.

According to Rallison,[13] a drop whose initial shape is spherical deforms into an ellipse whose principal axis is aligned with the flow direction in the shear flow, through a capillary number $Ca = \mu Sa/\gamma$, with increasing shear rate S, where μ is the viscosity of the suspending fluid, a is the drop size and γ is the surface-tension coefficient between the phases. The experimental isointensity curves which are elongated in the direction of ribbons, that of the shear flow, in lower q region, correspond to the scattering from the single particle elongated perpendicular to the shear flow, on the contrary. These features lead to the conclusion that the distorted scattering patterns do not arise from the particles deformed owing to the shear flow. Accordingly, the distorted patterns are considered to originate from the anisotropic interparticle interference effects, the maxima for the $Al_{92}V_3Fe_3Zr_2$ ribbons prepared with V_c values of 40 and 50 m/s, and are represented by the structure factor $S(q)$ in the eq. (1).

The TEM observation shows that the approximately spherical particles are precipitated in the $Al_{92}V_3Fe_3Zr_2$ alloy prepared with V_c of 40 m/s. Taylor[14] showed that small drops contained in another liquid suspension will hold nearly spherical under the shear flow, so long as shear rate S is small compared with $\sim 2\gamma/\mu_a$, and the shear S ruptures all droplets exceeding the break-up size $a_{burst} \propto \gamma/S\mu$. The radii of gyration evaluated in the Guinier approximation are plotted as a function of circumference velocity V_c of the melt-spinning roller in Fig. 11. The size of the precipitated particles decreasing with increasing V_c value was fitted to a good approximation, as shown in Fig. 11, with a hyperbolic curve a_1/S given by Taylor,[14] where a_1 is a parameter calculated by solving the nonlinear least squares problem. As the radius of gyration de-

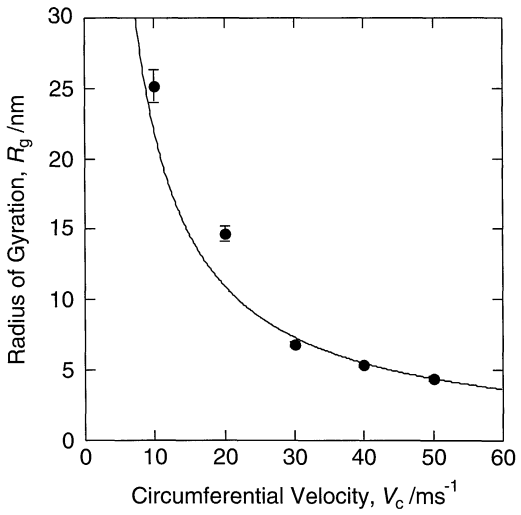

Fig. 11 Radius of gyration R_g versus circumferential velocity, along with the fitted hyperbolic curve $\sim 1/S$.

termined using the Guinier approximation is the z-average of the radii of gyration for a polydisperse system as recognized in many real systems, the Guinier approximation results in a larger value of the radius of gyration than the number-average for a polydisperse system, and the breakup size a_{burst} is considered to be able to represent the evaluated R_g values. The shear ruptures all precipitates exceeding the Taylor break-up size a_{burst} for the $Al_{92}V_3Fe_3Zr_2$ alloys.

Rayleigh developed the theory of the instability of long cylinders of fluid and showed that if the equilibrium surface $r = a$ is slightly deformed so as to become

$$r = a + \alpha \cos kz, \tag{4}$$

where z is measured along the axis, then the deformation is stable or unstable according to whether ka is greater or less than unity, or in other words, according to whether the wavelength λ is greater or less $2\pi a$, the circumference of the cylinder.[15] Rayleigh concluded that in the extreme where inertial effects of the material within the cylinder completely dominate those of external medium, the wavelength of maximum instability is given by[15]

$$\lambda = 4.51 \times 2a. \tag{5}$$

Seward, III observed in replica electron micrograph that the elongated particles in a lead borate glass produced by redrawing had disintegrated completely into rows of nearly spherical particles after 490°C heat-treatment for 40 min.[16] Although the electron micrograph showed not all particles in a given row of collinear spheres are of equal size nor spaced at uniform distance, he obtained a range of k values between about 3.5 and 7.5 by conservation of volume in some regions of the regularity.[16]

In the present case, the statistically averaged distance D between the particles can be estimated roughly from a relation $D \sim 2\pi/q_M$, where q_M is the position of a maximum in the scattered intensity, the deformed rings of diffuse maxima in the two-dimensional scattering data for the $Al_{92}V_3Fe_3Zr_2$ alloys prepared with V_c values of 40 and 50 m/s. The approximated values of the principal axes of the ellipse of the diffuse maxima are 0.21 ± 0.01 and $0.25 \pm 0.01\,nm^{-1}$ parallel and perpendicular to the direction of the ribbon, respectively, for the $Al_{92}V_3Fe_3Zr_2$ alloy prepared with V_c of 40 m/s (Fig. 8(a)), and are 0.22 ± 0.01 and $0.28 \pm 0.01\,nm^{-1}$ for 50 m/s yield the average distances D between the particles roughly: 29.9 ± 1.4 nm and 25.1 ± 1.0 nm parallel and perpendicular to the direction of the ribbons prepared with V_c of 40 m/s, and 28.6 ± 1.3 nm and 22.4 ± 0.8 nm for the ribbons prepared with 50 m/s. The ratio about 1.5 of the scattered intensity on the ellipse parallel to that perpendicular to the direction of the ribbon prepared with V_c of 40 m/s (Fig. 8(b)) shows that the precipitated particles are aligned to a considerable extent along the ribbon direction. Substituting values of $a_s = 6.9$ and 5.7 nm evaluated from the radii of gyration assuming spheres into eq. (5) from a ratio of a sphere to rod radius (for the cylindrical case) $a_s/a = 1.83$[16] yield values 34 and 29 nm for λ which are comparable to the estimated interparticle distances 30 and 29 nm along the ribbon direction for the $Al_{92}V_3Fe_3Zr_2$ alloy prepared with V_c values of 40 and 50 m/s, respectively. This estimation demonstrates that the elongated particles whose principal axis is aligned with the flow direction of the shear flow for the $Al_{92}V_3Fe_3Zr_2$ ribbons have disintegrated completely into rows of nearly spherical particles in the mode as described in the theory of the instability developed by Rayleigh.

The identification of the structural origins of the SAXS patterns is performed with the aid of the X-ray diffraction data, because this identification is impossible on the basis of SAXS data alone. According to Inoue *et al.*,[1] the microstructure in the $Al_{94.5}Cr_3Ce_1Co_{1.5}$ ribbons is formed by the solidification process of the primary precipitation of the I particles from liquid, followed by the precipitation of the remaining liquid as an Al phase. They also demonstrated that the nanoscale amorphous particles in coexistence with Al phase are formed in $Al_{94}V_4Fe_2$ alloys containing the solute elements V and Fe which lead to the suppression of the transition from super-cooled liquid to I-phase by the circumferential velocities of 40 and 50 m/s, and the same solidification process as that of the $Al_{94.5}Cr_3Ce_1Co_{1.5}$ ribbons was considered from the similarity of the microstructure and the formation of the disordered structure on the short-range scale in the nanoscale I particles.[3] In the case of the $Al_{92}V_3Fe_3Zr_2$ alloy, the same solidification process is also anticipated from the similar dependence of the X-ray diffraction patterns on the V_c value (Fig. 4). And the I particles or the nanoscale amorphous particles dispersed in a fcc-Al phase are considered to cause the SAXS patterns. Sizes of the precipitates calculated in the Guinier approximation are comparable to those obtained by the TEM measurements, and the origins of the SAXS patterns are the precipitates observed in the TEM measurements (Fig. 5).

Figure 12 shows the azimuthal dependence of the peak heights of the Bragg reflection from the (111) crystal planes of fcc-Al phase in the $Al_{92}V_3Fe_3Zr_2$ ribbons. The tendency for the (111) planes of fcc-Al to direct normal to the ribbon direction becomes strong with increasing the V_c value o 30 m/s. While, the directions of the (111) plane become random for the V_c values of 40 and 50 m/s. This result suggests some change in the precipitation mechanism for the preparation at the circumferential velocity V_c of 30 m/s, along with the

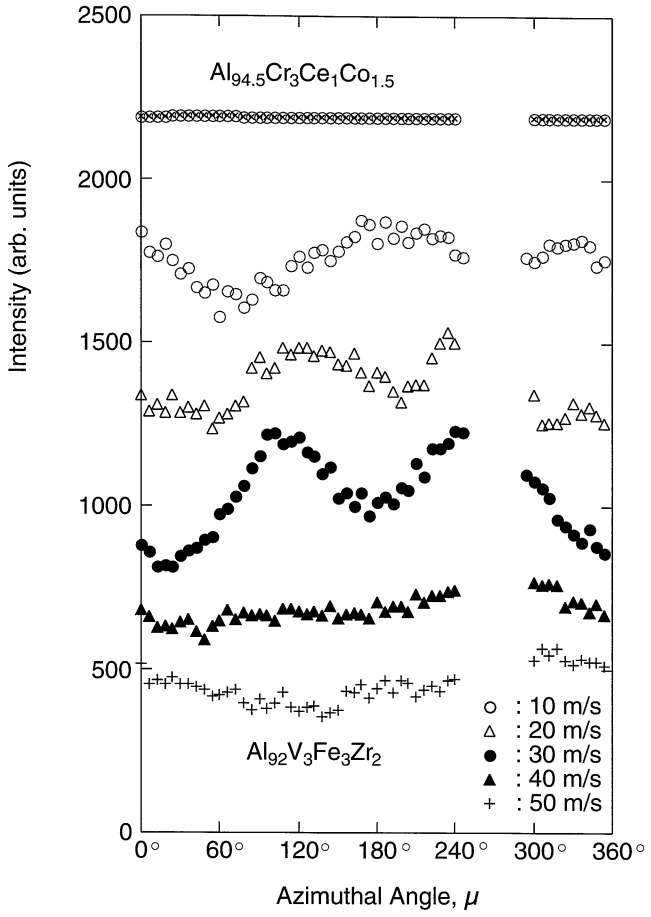

Fig. 12 Azimuthal peak heights of the Bragg reflection from the (111) crystal planes of fcc-Al phase in the melt-spun $Al_{92}V_3Fe_3Zr_2$ and $Al_{94.5}Cr_3Ce_1Co_{1.5}$ ribbons obtained from the diffraction data in Fig. 4.

SAXS results that the particles with a well-defined boundary are precipitated in an Al phase for the ribbons prepared only in the V_c region higher than 30 m/s.

5. Conclusions

Shear effects on the nucleation process have to be taken into account in the rapid solidification process of the $Al_{92}V_3Fe_3Zr_2$ ribbons prepared by the single roller melt-spinning technique with V_c values higher than 20 m/s. The shear brings about deformed patterns on two-dimensional isointensity SAXS curves of the $Al_{92}V_3Fe_3Zr_2$ alloy prepared with V_c values higher than 20 m/s. The deformed patterns extend towards higher q regions and the structure becomes to deform on shorter range scales, with increasing V_c value, that is, the shear rate. At the same time, the formation of the nanoscale amorphous particles in coexistence with an Al phase is observed for the $Al_{92}V_3Fe_3Zr_2$ alloy prepared with V_c values higher than 30 m/s.

The precipitates decrease in size with increasing V_c value from 10 to 50 m/s, which can be interpreted in terms of the description that all precipitates exceeding the Taylor break-up size R_{burst} are ruptured by shear. The ruptured particles are aligned with the ribbon direction with interparticle spacing 30 nm for the ribbon prepared with the circumferential velocity 40 m/s, and the interparticle spacing decreases to 29 nm with increasing the velocity from 40 to 50 m/s. Good agreement between the spacings evaluated from the SAXS data and those calculated from the instability theory developed by Rayleigh is considered to lead to the precipitation mechanism in shear that the elongated particles whose principal axis is aligned with the flow direction by the shear flow have disintegrated completely into rows of nearly spherical particles.

The SAXS patterns for the $Al_{92}V_3Fe_3Zr_2$ alloy prepared with V_c higher than 30 m/s are characteristic of the scattering from particles with a well-defined boundary precipitated in an medium, while the patterns for the $Al_{92}V_3Fe_3Zr_2$ alloy prepared with V_c less than 20 m/s and the $Al_{94.5}Cr_3Ce_1Co_{1.5}$ alloy show the absence of distinct interface. This SAXS result indicates some change in the precipitation mechanism for the preparation with V_c of 30 m/s, along with the azimuthal dependence of the peak heights from the (111) crystal planes of fcc-Al phase in the $Al_{92}V_3Fe_3Zr_2$ ribbons.

In the case of $Al_{94.5}Cr_3Ce_1Co_{1.5}$ ribbon prepared with a V_c value of 40 m/s, where an isotropic SAXS pattern was observed, the nanosized clusters of a quasi-crystalline phase have been known to form with high growth rate.[3] The formation of the nanoscale amorphous particles through the suppression of the transition from super-cooled liquid to I-phase and the deformed SAXS patterns in the $Al_{92}V_3Fe_3Zr_2$ ribbons are considered to result from the retardation of the diffusivity of the solute elements vanadium and iron.

REFERENCES

1) *e.g.* A. Inoue, H. M. Kimura, K. Sasamori and T. Masumoto: Mater. Trans., JIM **35** (1994) 85–94.
2) A. Inoue and T. Masumoto: Keikinzoku **42** (1992) 299–305.
3) A. Inoue, H. M. Kimura, K. Sasamori and T. Masumoto: Nanostruct. Mater. **7** (1996) 363–382
4) S. Kavesh: *Metallic Glasses*, (American Society for Metals, 1977) pp. 36–73.
5) D. J. Evans, H. J. M. Hanley and S. Hess: Phys. Today **37**(1) (1984) 26–33.
6) R. F. Bruinsma and C. R. Safinya: Phys. Rev. A **43** (1991) 5377–5404.
7) *e.g.* A. Onuki: J. Phys.: Condens Matter **9** (1997) 6119–6157.
8) W. I. Goldburg and K. Y. Min: Physica A **204** (1994) 246–260.
9) A. Guinier and G. Fournet: *Small-angle scattering of X-rays*, (John Wiley & Sons, NY, 1955).
10) T. Kamiyama, H. M. Kimura, K. Sasamori and A. Inoue: Scr. Metall. in printing.
11) T. Nakagawa and Y. Oyanagi: *Recent Developments in Statistical Interference and Data Analysis*, ed. by K. Matusita (North Holland Publishing Company, Amsterdam, 1980) pp. 221–225.
12) H. Schlichting: *Binary Layer Theory.* (McGraw-Hill, NY, 1972).
13) J. M. Rallison: Ann. Rev. Fluid Mech. **16** (1984) 45-66.
14) G. I. Taylor: Proc. Roy. Soc. **138A** (1932) 41–48.
15) Lord Rayleigh: Philos. Mag. **34** (1892) 145–154, 177–180.
16) T. P. Seward, III: J. Non-Cryst. Solids **15** (1974) 487–504.